Ionospheric response to the X-class solar flare on 7 September 2005

Bo Xiong,[1,2,3] Weixing Wan,[1] Libo Liu,[1] Paul Withers,[4] Biqiang Zhao,[1] Baiqi Ning,[1] Yong Wei,[5] Huijun Le,[1] Zhipeng Ren,[1] Yiding Chen,[1] Maosheng He,[1,2] and Jing Liu[1,2]

[1]   We investigate the extreme ionospheric effect during the intense solar flare (X17.0/3B) that occurred on 7 September 2005. A strong E region electron density enhancement is observed by the incoherent scatter radars at Millstone Hill, Sondrestrom, and Tromsø, as well as by the radio occultation experiment on board the CHAMP satellite. The observations from both Millstone Hill and Sondrestrom stations show the average percentage enhancements of electron density during 17:40–18:10 UT are more than 200% near the E region peak height but only about 10% near the F region peak height; as a result, it leads to an unusual phenomenon that the E region electron density exceeds the F region electron density. We ascribe the unusual response to weak enhancement in EUV flux and strong enhancement in X-ray flux during this flare. To further understand this unusual feature, we analyze in detail the E region response by comparing the electron production rates derived from the measurements with those fitted by the Chapman production function. Our results demonstrate that the Chapman production theory fits the observations better in the flare time than in the nonflare time, which is attributed to the obvious difference in the solar radiation spectra at flare and nonflare times. Owing to the strong enhancement in X-ray flux during this flare, the E region electron production is more dominated by the X-ray, and the Chapman ionization theory is more applicable in the flare time than in the nonflare time. In addition, we propose a method to estimate the effective solar radiation flux from the ionospheric observations of electron density profiles. The radiation flux derived with our method agrees well with the X-ray flux at 0.1–0.8 nm observed by GOES-12.

Citation: Xiong, B., et al. (2011), Ionospheric response to the X-class solar flare on 7 September 2005, *J. Geophys. Res.*, *116*, A11317, doi:10.1029/2011JA016961.

1.   Introduction

[2]   The ionospheric response to solar flares is not only an important classical topic for solar-terrestrial relations, but also a focus of current space weather research [e.g., *Woods et al.*, 2003]. Since 1960s, researchers have studied many kinds of sudden ionospheric disturbances, such as sudden frequency deviation [e.g., *Donnelly*, 1969; *Liu et al.*, 1996], short wave fadeout [*Stonehocker*, 1970], sudden phase anomaly [*Ohshio*, 1971], and sudden increase of total electron content (SITEC) [e.g., *Garriott et al.*, 1967; *Mendillo et al.*, 1974; *Afraimovich et al.*, 2001; *Leonovich et al.*, 2002; *Wan et al.*, 2005; *Zhang and Xiao*, 2005; *Liu et al.*, 2006; *Mahajan et al.*, 2010]. Meanwhile, there have been some comparative studies dealing with the ionospheric response to solar flares on different planets [e.g., *Mendillo et al.*, 2006].

[3]   The altitude distribution of the ionospheric response to solar flares is a noticeable and interesting issue. To study the effect of flares on electron density profiles, two kinds of ground-based instruments, ionosonde and incoherent scatter (IS) radar, are the main candidates. Owing to the short wave fadeout effects, ionosondes can rarely record complete ionograms during flares [e.g., *Mendillo et al.*, 2006; *Smithtro et al.*, 2006; *Manju et al.*, 2009]. Thus IS radar is the only type of ground-based instrument used in the study of the altitude distribution of the ionospheric response, as noticed by *Thome and Wagner* [1971] and *Mendillo and Evans* [1974]. These authors reported electron density enhancements in both E and F regions during some solar flares, and found that the relative response is stronger in the E region than in the F region. Meanwhile, some simulations have studied the flare effects at different altitudes. *Le et al.* [2007] simulated the

[1]Beijing National Observatory of Space Environment, Institute of Geology and Geophysics, Chinese Academy of Sciences, Beijing, China.
[2]Graduate University of Chinese Academy of Sciences, Beijing, China.
[3]Department of Mathematics and Physics, North China Electric Power University, Baoding, China.
[4]Center for Space Physics, Boston University, Boston, Massachusetts, USA.
[5]Max-Planck-Institut für Sonnensystemforschung, Katlenburg-Lindau, Germany.

Table 1. Details of the Data Sets Used in This Study

Instrument	Observation Time (UT)	Geographic Longitude, Latitude (deg)	Parameters
GOES-12/X-Ray Sensor	16:20–19:35	−74.50, 0	Flux integrated at 0.1–0.8 nm
TIMED/Solar EUV Experiment	17:00	−47.61, −4.28	Flux at 0–195 nm
	18:37	−72.16, −4.63	
IS Radar	16:20–19:35	−71.50, 42.60 (Millstone Hill)	Electron density; Electron temperature
		−50.95, 66.99 (Sondrestrom)	
		19.23, 69.59 (Tromsø)	
CHAMP/GPS Receiver	16:39	−76.92, 45.98	Electron density
	16:46	−80.09, 71.59	
	17:41	−87.20, −71.42	
	17:47	−114.47, −51.88	
	18:06	−106.30, 27.76	
	19:12	−126.75, −75.29	
	19:19	−137.50, −48.51	

altitude distribution of the ionospheric response to solar flares and showed that the largest relative increase in electron density is around 300% in the E region at ~115 km altitude. Utilizing the flare irradiance spectral model (FISM) and the thermosphere-ionosphere-mesosphere electrodynamics general circulation model (TIME-GCM), *Qian et al.* [2010] calculated the ionospheric response to two X17 flares which occur at the center and near the limb of the solar disk. They found that the enhancements of ionospheric production rate, loss rate and electron density above ~120 km are all stronger for the flare at the solar disc center than for that near the solar limb region.

[4] The flare's location on solar disc is an important aspect in the research of the ionospheric response to solar flares. *Zhang et al.* [2002] analyzed the correlation between SITEC and the flare's location on solar disc. They found that the flares with the same X-ray level produce a stronger ionospheric response if they have a smaller central meridian distance (CMD). *Tsurutani et al.* [2005] examined the ionospheric effects during the X17.2 flare on 28 October 2003 (CMD = 8°) and the X28 flare on 4 November 2003 (CMD = 83°). The latter solar flare has less EUV flux and induces a weaker ionospheric response. They attributed this phenomenon to the limb effect of the flare's location on the solar disc. By calculating the increases in total electron content (TEC) during some M2.0–M5.7 solar flares, *Leonovich et al.* [2010] showed that the amplitude of ionospheric TEC response to solar flares increases with decreasing distance from the central solar meridian.

[5] The studies mentioned above show a significant limb effect on the ionospheric response to solar flares, which focuses on the behaviors of integral electron density on the basis of the GPS TEC data. In this study, our intention is to investigate the altitude distribution of the ionospheric response to the significant limb solar flare which occurred on 7 September 2005, with a class of X17 and a CMD of 77°. We collected electron density profiles measured by three IS radars and the CHAMP satellite and conducted an analysis of the ionospheric response to the flare, particularly the electron density and electron production rate responses in the E region. In the following sections, we will first introduce the observations during the intense flare and initial findings. Then we give results of an analysis based on derivation of the flare-induced electron production rate. Next, further discussions regarding to the derived results are pro-

vided. Finally, a summary is presented for the main properties of the ionospheric response to the flare.

2. Observation and Initial Results

[6] On 7 September 2005, a very intense solar flare (X17.0) occurred near the east limb of the solar disk (11°S, 77°E). Multiple data sets are used to explore the ionospheric response to this intense flare and the details of these data sets are shown in Table 1. As observed by GOES-12 in the X-ray wavelength band from 0.1 to 0.8 nm (see Figures 2, 6, or 7), the flare started at 17:17 UT and reached the maximum intensity at 17:40 UT. The peak to preflare ratio of X-ray flux reaches 2180, from the quiet level of 7.8×10^{-7} W/m^2 to its peak value of 1.7×10^{-3} W/m^2. The Solar EUV Experiment (SEE) [*Woods et al.*, 2005] instrument aboard the Thermosphere, Ionosphere, Mesosphere, Energetics, and Dynamics (TIMED) spacecraft measured the preflare and flare solar irradiance at 0–195 nm at 17:00 and 18:37 UT, respectively. The increase in solar irradiance is much greater at 0–20 nm than at 20.5–195 nm during the flare. The maximum enhancement is more than a factor of 44 at 0–20 nm, but only about 48% at 20.5–195 nm.

[7] To study the flare-induced ionospheric response, we analyze the observations of three IS radars, which are located at Millstone Hill (42.60°N, 71.50°W; Geomagnetic Latitude 52.53°N), Sondrestrom (66.99°N, 50.95°W; 72.95°N) and Tromsø (69.59°N, 19.23°E; 66.40°N), as shown in Figure 1. Figure 1 illustrates the solar zenith angles (black bold contours) at 17:40 UT when the X-ray flux of the flare reached its maximum. Meanwhile, seven electron density profiles measured by the radio occultation experiment aboard the CHAMP satellite are collected and the corresponding locations (blue pentagrams) are also shown in Figure 1.

[8] Figure 2 illustrates the electron density measurements of the three IS radars during the intense solar flare. From top to bottom, Figure 2 shows the electron density distribution observed from Millstone Hill, Sondrestrom, and Tromsø. From left to right, Figure 2 shows the observed electron density on the reference day, the flare day, and their differences. Here we choose 5 September (Kp = 2.3) as the reference day from which to find the electron density deviations caused by the flare. For comparison, the X-ray flux from GOES-12 is superimposed. To show clearly the flare
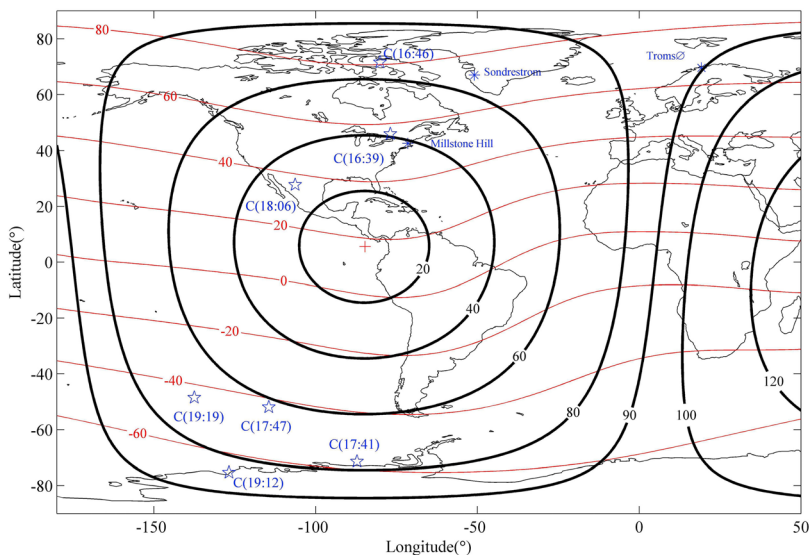
Figure 1. Geographic coordinates of three IS radars (blue asterisks), time (UT) and locations (blue pentagrams) observed by the CHAMP satellite, geomagnetic latitudes (red solid lines), and solar zenith angles (solid black contours) at 17:40 UT.

effect on the E region ionosphere, the white rectangles indicate the response of electron density near the E region peak height and around the peak time of X-ray flux.

[9] As shown in Figure 2, the E region electron density enhancements are remarkable during the flare at the three stations, particularly at Millstone Hill and Sondrestrom stations. Furthermore, the electron density is clearly larger in the E region than in the F region at the two stations. The phenomenon of E region electron density exceeding F region electron density during a solar flare has not been
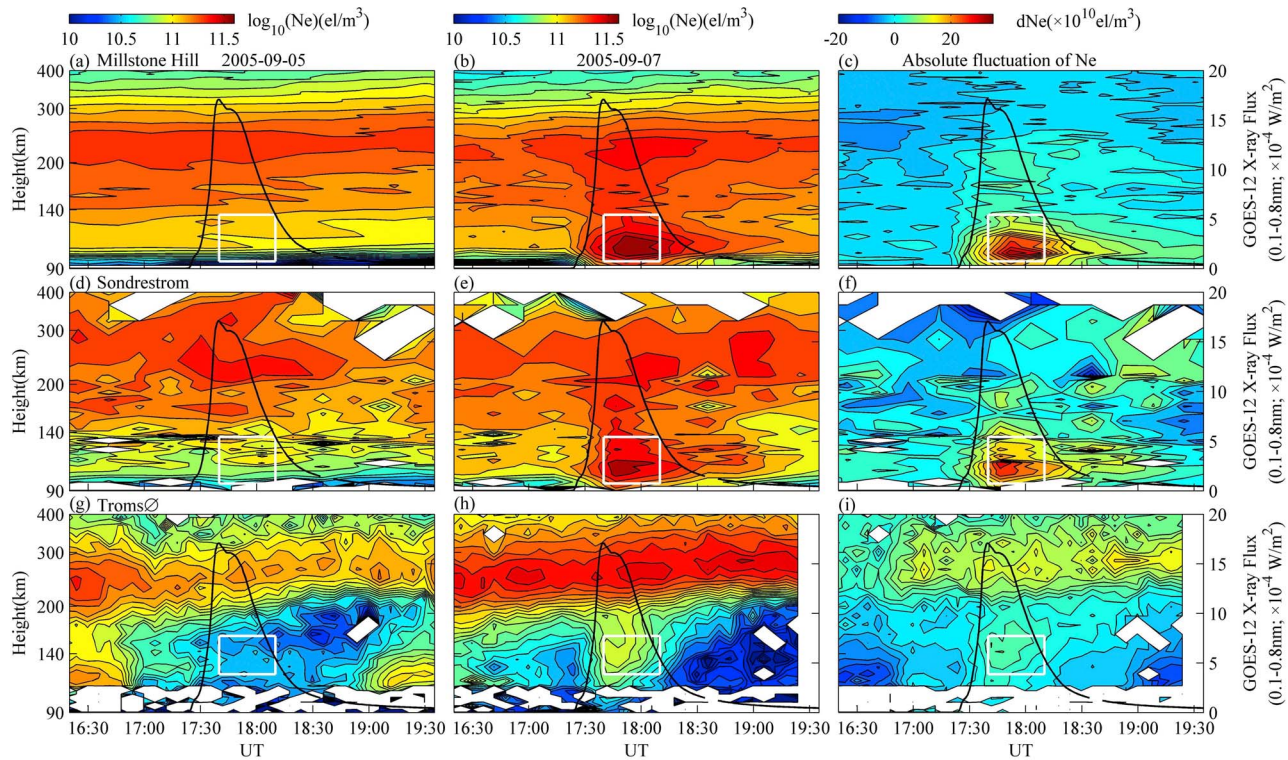
Figure 2. (a and b) Electron density distributions during 16:20–19:35 UT on the reference and flare days in Millstone Hill. (c) Absolute deviation of electron density between the flare and reference days in Millstone Hill. (d–f) Same as Figures 2a–2c but for Sondrestrom. (g–i) Same as Figures 2a–2c but for Tromsø. Black curves indicate the X-ray flux observed by GOES-12. White rectangles show the flare effect of ionosphere near the E region peak height and around the peak time of X-ray flux.
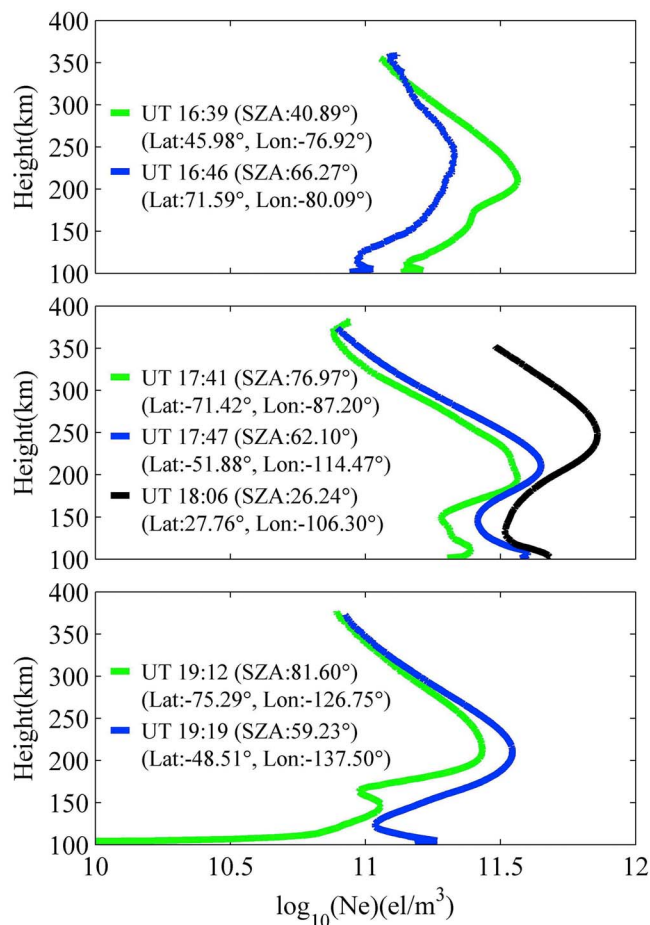
Figure 3. Electron density profiles measured by the CHAMP satellite during 16:20–19:35 UT on the dayside.

reported before. To further understand the E region electron density enhancement during this flare, we inspect the absolute and percentage differences in electron density between the flare and reference days. During the flare, the absolute enhancements of electron density in the E region are more obvious than those in the F region at Millstone Hill and Sondrestrom, as shown in Figures 2c and 2f. The absolute enhancement in the E region at Tromsø (Figure 2i) is also obvious although not stronger than that in the F region. The average percentage enhancements of electron density during 17:40–18:10 UT are 218%, 232% and 130% near the E region peak height and 9%, 11% and 78% near the F region peak height in Millstone Hill, Sondrestrom and Tromsø, respectively. The relative enhancements in the E region are obviously stronger than those in the F region for the three stations. This result is similar to previous reports [e.g., *Thome and Wagner*, 1971].

[10] During this flare, the CHAMP satellite traveled from the southern to northern hemisphere and recorded the ionospheric response to this intense flare at different locations and different times, as shown in Figure 3. From top to bottom, Figure 3 depicts the electron density profiles recorded before, during, and after the flare. We mark the time (UT), solar zenith angle (SZA), and location for each profile. As shown in Figure 3, the sudden enhancements of electron density in the E region are also seen in the obser-

vations of the CHAMP satellite during the flare. Furthermore, the electron density in the E region is larger at smaller SZA. At 17:47 UT, the magnitude of the electron density observed by CHAMP in the E region is comparable to that in the F region. The peak electron density is 3.99×10^{11} el/m^3 in the E region and 4.47×10^{11} el/m^3 in the F region. The difference in electron density is only 0.48×10^{11} el/m^3.

3. Flare-Induced Electron Production

[11] Owing to the sudden enhancement of solar radiation during the flare, the electron density production is the most important factor for the ionospheric variation. In this section, we study the behavior of the flare-induced electron production according to the continuity equation and Chapman ionization theory.

3.1. Method of Analysis

[12] As well known, the variation rate of electron density $\partial Ne/\partial t$ is affected by the electron density production, loss and transport rates in the continuity equation. Because the flare explosion is a very rapid process, its effect on the transport can be ignored in continuity equation [e.g., *Wan et al.*, 2005], especially at the E region altitudes. Therefore the E region continuity equation is expressed as,

$$\partial Ne/\partial t = Q - \alpha Ne^2, \qquad (1)$$

where Q represents the production rate of the electron density, α is the recombination constant, and Ne is the electron density. The value of α is calculated on the basis of the electron temperature and the ion densities (O_2^+, NO^+). The electron temperature is obtained from the observation of IS radars or the International Reference Ionosphere (IRI)-2000 model (for the CHAMP satellite). The ion concentrations are taken from the IRI-2000 model. Ne is measured by IS radars or CHAMP satellite. By analyzing the observational data of the IS radars, we find that the absolute value of $\partial Ne/\partial t$ is much smaller than that of the electron loss rate (αNe^2) below 200 km during this flare. Therefore, we can obtain the production rate of the electron density

$$Q = \alpha Ne^2, \qquad (2)$$

which is considered as the observed production rate.

[13] According to Chapman ionization theory, Q takes the form of Chapman function, which is a function of altitude h, atmosphere scale height H and SZA χ [*Rishbeth and Garriott*, 1969],

$$Q = \frac{\eta I_\infty(t)}{eHch(\chi)} \exp\left(1 - \frac{h-hm}{H} - e^{-\frac{h-hm}{H}} \right), \qquad (3)$$

where η represents the efficiency of ionospheric ionization; I_∞ is the radiation flux of solar at the top of atmosphere; hm is the reference height where the production rate is the largest; ch is the Chapman's grazing incidence function [*Smith and Smith*, 1972]. In equation (3), H is calculated by the NRLMSIS-00 model. By fitting the observed production rate (αNe^2) with the Chapman production function as shown in equation (3), we can retrieve the effective solar radiation flux ηI_∞ and the height of the largest electron production rate hm, and then obtain the fitted production rate.
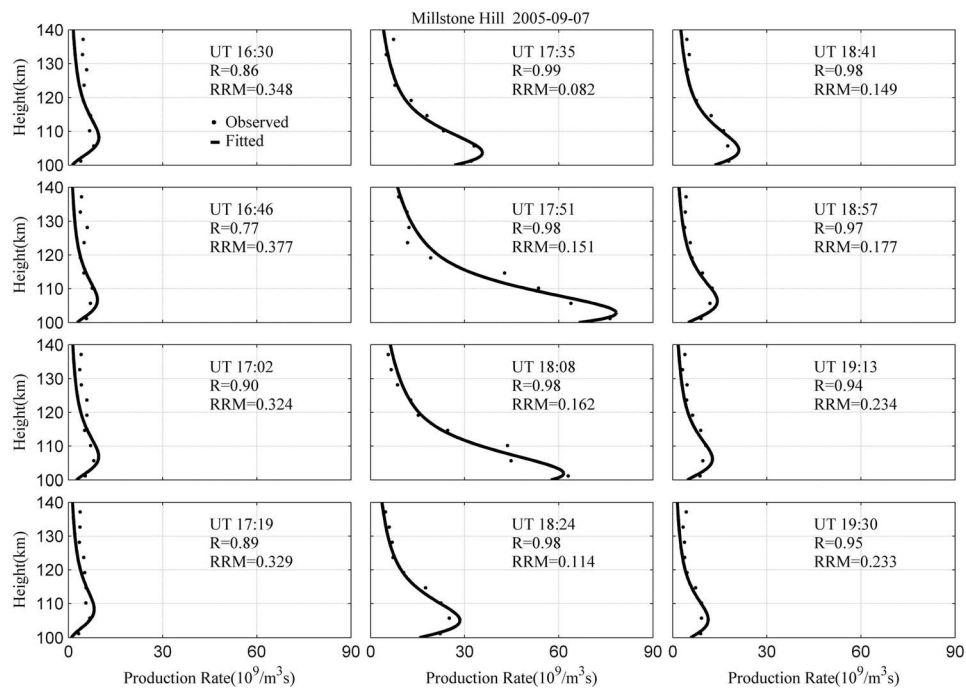
Figure 4. A comparison of the fitted and observed electron production rates between 16:20 and 19:35 UT in Millstone Hill.

3.2. Results

[14] Figures 4 and 5 illustrate the observed and fitted electron production rates at 100–140 km in Millstone Hill and Sondrestrom. Figures 4 and 5 show the observation time, the correlation coefficient of the fitted and observed electron production rates, and the Ratio of the Root-mean-square error (between the fitted and observed electron pro-

duction rates) to the Mean value of observed production rate (RRM). As shown in Figures 4 and 5, the response of the electron production rate to the solar flare is clearly seen in Millstone Hill and Sondrestrom. The production rate increases obviously at the onset of the flare and gradually returns to its preflare level after 18:55 UT. Meanwhile, Figures 4 and 5 illustrate a good correlation between the
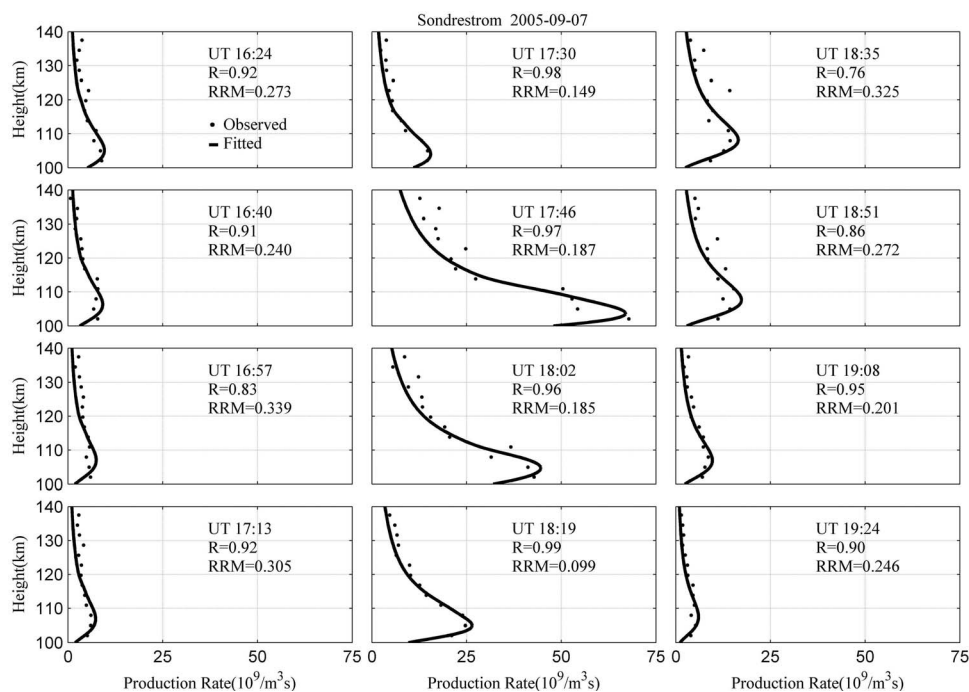
Figure 5. Similar to Figure 4 but for Sondrestrom.
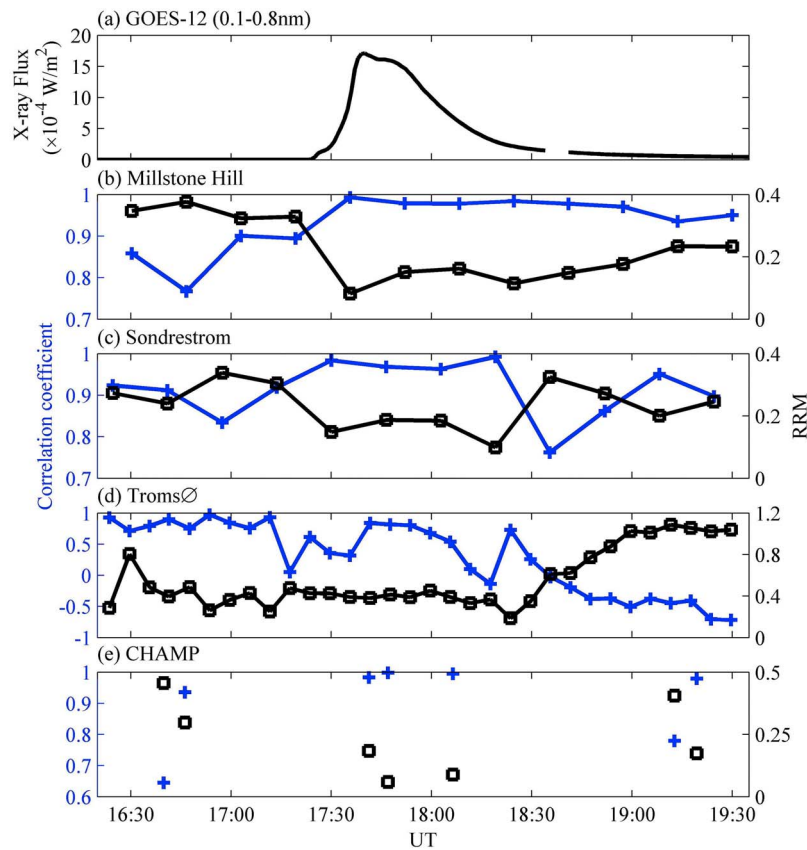
Figure 6. (a) Temporal variation of the X-ray flux measured by GOES-12. (b–e) Temporal evolutions of the correlation coefficient (between the fitted and observed electron production rates) and RRM for three IS radars and the CHAMP satellite. Blue pluses and black squares indicate the correlation coefficients and RRM, respectively.

fitted and observed production rates. The correlation coefficients in the two stations are larger than 0.75 during 16:20–19:35 UT. During the flare, the coefficients increase obviously and are as high as 0.99. From Figures 4 and 5, we find that the correlations during the flare are better than those before and after the flare. Furthermore, the RRMs decrease remarkably during the flare in the two stations. This indicates that Chapman production theory fits the observations better in the flare time than in the nonflare time. An explanation for this behavior is discussed in a later section.

[15] In Figure 6 the temporal evolutions of the correlation coefficient and RRM are shown for three IS radars (Figures 6b–6d) and the CHAMP satellite (Figure 6e) between 16:20 UT and 19:35 UT. For comparison, the X-ray flux measured by GOES-12 is displayed in Figure 6a for the corresponding period. In Figures 6b, 6c, and 6e, the correlation coefficients increase and RRMs decrease for Millstone Hill, Sondrestrom and CHAMP satellite when the X-ray flux increases. Around the peak of the X-ray flux, the correlation coefficients and RRMs are near 0.97 and 0.16, respectively. In Figure 6d the temporal evolutions of the correlation coefficient and RRM at Tromsø are dominated by the sunset effect as well as the flare effect. Before the start of the flare, the correlation coefficients decrease and RRMs increase. At the onset of the solar flare, the correlation coefficients remain near 0.7 and the RRMs remain near 0.35 until 18:10 UT. When the sunset effect is stronger compared with the flare

effect, the RRMs increase quickly and the positive correlation decreases, which indicates the Chapman production function cannot well describe the electron production rate when SZA > 90° after 18:10 UT. From the temporal evolutions of the correlation coefficient and RRM for three IS radars and the CHAMP satellite, we find that Chapman ionization theory is more applicable during the flare than in the nonflare time.

[16] Figure 7 presents the temporal variation of the effective solar radiation fluxes for three IS radars and the CHAMP satellite according to equation (3). In Tromsø, the effective solar radiation flux is only shown before 18:10 UT because the Chapman production function cannot well describe the electron production rate when SZA > 90° after 18:10 UT. The X-ray flux from GOES-12 is superimposed in Figure 7. To further understand the relationship between the effective solar radiation flux and the X-ray flux, their correlation coefficients are given in Figure 7. For three IS radars and the CHAMP satellite, the effective solar radiation fluxes start to increase obviously after the onset of the flare, reach the maximum intensity near 17:40 UT, and gradually recover to the preflare state with the decrease of the X-ray flux. The temporal evolutions of effective solar radiation fluxes have the same trend and are very consistent with that of the X-ray flux. Meanwhile, the values of the two kinds of fluxes are the same in magnitude near the peak of X-ray flux. In addition, the correlation coefficients between the effective
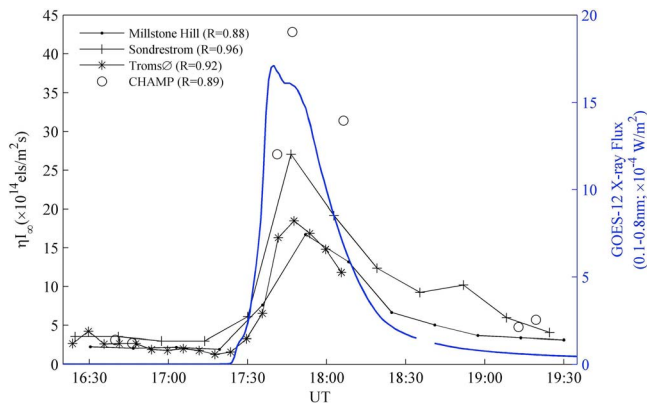
Figure 7. Temporal evolution of the effective solar radiation fluxes obtained from the observations of three IS radars and the CHAMP satellite. Blue curve indicates the X-ray flux measured by GOES-12.

solar radiation flux and the X-ray flux are all greater than 0.85. Since the X-ray flux is an important portion of the solar radiation affecting the electron production rate in the lower ionosphere, the good correlation indicates that the derived effective solar radiation flux can well represent the actual solar radiation. Thus, the method used to estimate the effective solar radiation flux from the ionospheric observations may have potential applications for studying the solar radiation. This makes it possible to extend the temporal range of solar radiation studies to the periods when satellite and rocket measurements were not conducted and study long-term variations in solar radiation. Meanwhile, the effective solar radiation flux estimated from the real-time ionospheric observations may represent the current solar radiation and can be further used to monitor space weather [e.g., *Nusinov*, 2006; *Liu et al.*, 2011].

4. Discussion

[17] The measurements in Millstone Hill and Sondrestrom show larger electron density in the E region than in the F region during the limb solar flare on 7 September 2005. Several previous workers have used measurements from IS radars (23 May 1967 and 7 August 1972) to study the altitude distribution of solar flare effects on the ionosphere [*Thome and Wagner*, 1971; *Mendillo and Evans*, 1974]. Their results also showed a significant electron density enhancement in the E region, while the E region peak electron density (NmE) remained lower than the F_2 region peak electron density (NmF$_2$). To obtain larger electron density in the E region than in the F region during a solar flare, two conditions are needed: the ionization source for the F region (EUV) is weakly enhanced, which limits the electron density increase in this region, and the ionization source for the E region (X-ray) is strongly enhanced, which causes large electron density increase in this region. The solar flare on 7 September 2005 just satisfies the two conditions. First, this is a limb flare with CMD = 77°, which would cause little increase in EUV bands of 17–91 nm and consequently small increase in NmF$_2$ [*Donnelly*, 1976; *Tsurutani et al.*, 2005; *Zhang et al.*, 2011]. Second, this is a great flare with a class of X17, which would cause large

enhancement in X-ray bands and consequently great enhancement in NmE [*Qian et al.*, 2010]. For the solar flares on 23 May 1967 and 7 August 1972 studied by previous workers, the optical classes of the two events are 2B and 3B, and their CMD values are about 25° and 37°. The measurements show that the electron density in the E region does not exceed that in the F region, which may be because the two flare events are not limb events and their X-ray radiation is not strongly enhanced. On 4 November 2003, the greatest flare of class X28 with CMD = 83° satisfies the above two conditions. The unusual phenomenon that the E region electron density exceeds the F region electron density may have occurred. Unfortunately, the lack of observations of IS radars prevents us from testing this hypothesis.

[18] At Tromsø, the E region electron density does not exceed the F region density during this flare. The behavior of the ionosphere at Tromsø is different from that in Millstone Hill and Sondrestrom, which is caused by the SZA difference. At the peak time of X-ray flux, the Tromsø station is around the terminator. *Zhang et al.* [2006] found the peak of electron production rate in the F region is larger than that in the E region when SZA is larger than 90°. In the modeling study, *Le et al.* [2007] showed that around sunrise and sunset the largest flare effect does not occurs at ~110 km as that in the daytime, but at higher altitudes (e.g., 190 km for an equinox flare).

[19] The results in section 3 reveal that the Chapman production theory fits the observations better in the flare time than in the nonflare time, which results from the difference in the solar spectrum. As well known, the contribution to E region production mainly comes from the X-ray (0.8–14 nm) and EUV (80–102.7 nm) regions in the absence of flares [e.g., *Rishbeth and Garriott*, 1969; *Nusinov*, 2006]. By modeling the ionization rates under moderate solar activity condition at SZA 45°, *Qian et al.* [2010] found that the ionization peak in the E region is dominated by the solar irradiance at 0.05–23 nm and 102.57 nm. The above viewpoints indicate that the solar radiation over a broad wavelength range affects the E region electron production rate under nonflare activity condition.

[20] However, the E region electron production rate is dominated by the solar radiation over a limited spectral range during the flare because the flare-induced enhancement is much stronger in X-ray flux than in EUV flux. *Woods et al.* [2004] reported that the ratios of the flare irradiance to the preflare irradiance are 570 and 42 as separately observed by GOES (0.1–0.8 nm) and the Solar Radiation and Climate Experiment (SORCE) spacecraft (0.1–7 nm), while the EUV irradiance (27–115 nm) increases by a factor of 2 as measured by the TIMED spacecraft during the X17.2 flare on 28 October 2003. *Leonovich et al.* [2010] constructed a model of the disturbed flare spectrum at 0.1–105 nm for the 14 July 2000 flare. They reported that the flare to nonflare radiation flux ratios are 1000 at 0.1–0.8 nm and 1.3 at 10–105 nm. During this flare, the X-ray flux enhancement is also much stronger than that in EUV flux. Figure 8 illustrates the flare to preflare solar irradiance spectrum ratio at 0–195 nm measured by the TIMED SEE instrument on 7 September 2005. The flare spectrum is measured 57 min after the X-ray flare peak observed by GOES-12, and its preflare spectrum is taken near 17:00 UT. To show clearly the variation of the spectrum affecting the
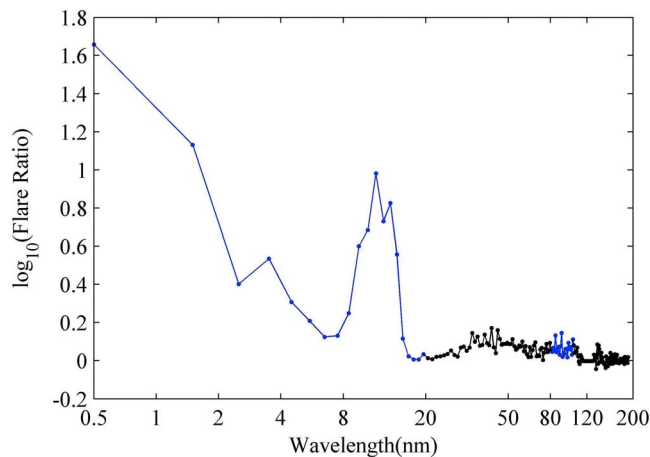
Figure 8. Flare to preflare solar irradiance ratio in the 0–195 nm wavelength range measured by TIMED SEE. Blue curves indicate the flare ratios in the 0–20 and 80–103 nm wavelength ranges.

electron production rate in the lower ionosphere, the blue curves in Figure 8 indicate the flare ratios in the 0–20 nm and 80–103 nm wavelength ranges. As shown in Figure 8, the increase is very strong in the 0–4 nm and 9–15 nm wavelength ranges, but not obvious in the 80–103 nm range. Because TIMED observed the flare a few minutes after the X-ray flare peak, the maximum variations in the 0–4 nm and 9–15 nm ranges are expected to be larger than those measured by TIMED. Owing to the strong enhancement in X-ray flux and the weak enhancement in EUV flux during this flare, the contribution of the X-ray flux variation to the increase for the *E* region electron production rate is more than that of EUV flux variation. As a result, the *E* region electron production during the flare is more dominated by the X-ray than that in the nonflare time, and the Chapman production theory is more applicable in the flare time than in the nonflare time.

5. Summary

[21] We have used the data from three IS radars and the CHAMP satellite to study the ionospheric response to the solar flare on 7 September 2005. The major findings are summarized as follows.

[22] 1. The flare-induced *E* region electron density is larger than that in the *F* region at Millstone Hill and Sondrestrom. Our investigations show that the unusual feature is mainly attributed to weak enhancement in EUV flux and strong enhancement in X-ray flux during this flare.

[23] 2. Chapman production theory fits the observations better in the flare time than in the nonflare time. This results from the different dominant spectra in solar radiation at flare and nonflare times.

[24] 3. On the basis of ionospheric observations of electron density profiles, a method is proposed to estimate the effective solar radiation flux. The radiation flux derived with the method is in good agreement with the X-ray flux at 0.1–0.8 nm observed by GOES-12 during this flare. The method may have potential applications for studying solar radiation.

[25] In addition, these observations during this flare offer new opportunities to test and validate existing models, especially for the detailed spectrum of solar radiation and the importance of flare's location on solar disc.

References

Afraimovich, E. L., A. T. Altynsev, E. A. Kosogorov, N. S. Larina, and L. A. Leonovich (2001), Ionospheric effects of the solar flares of September 23, 1998 and July 29, 1999 as deduced from global GPS network data, *J. Atmos. Sol. Terr. Phys.*, *63*, 1841–1849, doi:10.1016/S1364-6826(01)00060-8.

Donnelly, R. F. (1969), Contribution of X-ray and EUV bursts of solar flares to sudden frequency deviations, *J. Geophys. Res.*, *74*, 1873–1877, doi:10.1029/JA074i007p01873.

Donnelly, R. F. (1976), Empirical models of solar flare X-ray and EUV emissions for use in studying their *E* and *F* region effects, *J. Geophys. Res.*, *81*, 4745–4753, doi:10.1029/JA081i025p04745.

Garriott, O. K., A. V. da Rosa, M. J. Davis, and D. G. Villard Jr. (1967), Solar flare effects in the ionosphere, *J. Geophys. Res.*, *72*, 6099–6103, doi:10.1029/JZ072i023p06099.

Le, H., L. Liu, B. Chen, J. Lei, X. Yue, and W. Wan (2007), Modeling the responses of the middle latitude ionosphere to solar flares, *J. Atmos. Sol. Terr. Phys.*, *69*, 1587–1598, doi:10.1016/j.jastp.2007.06.005.

Leonovich, L. A., E. L. Afraimovich, E. B. Romanova, and A. V. Taschilin (2002), Estimating the contribution from different ionospheric regions to the TEC response to the solar flares using data from the international GPS network, *Ann. Geophys.*, *20*, 1935–1941, doi:10.5194/angeo-20-1935-2002.

Leonovich, L. A., A. V. Taschilin, and O. Y. Portnyagina (2010), Dependence of the ionospheric response on the solar flare parameters based on the theoretical modeling and GPS data, *Geomagn. Aeron.*, *50*, 201–210, doi:10.1134/S0016793210020076.

Liu, J. Y., C. S. Chiu, and C. H. Lin (1996), The solar flare radiation responsible for sudden frequency deviation and geomagnetic fluctuation, *J. Geophys. Res.*, *101*, 10,855–10,862, doi:10.1029/95JA03676.

Liu, J. Y., et al. (2006), Solar flare signatures of the ionospheric GPS total electron content, *J. Geophys. Res.*, *111*, A05308, doi:10.1029/2005JA011306.

Liu, L., W. Wan, Y. Chen, and H. Le (2011), Solar activity effects of the ionosphere: A brief review, *Chin. Sci. Bull.*, *56*, 1202–1211, doi:10.1007/s11434-010-4226-9.

Mahajan, K. K., N. K. Lodhi, and A. K. Upadhayaya (2010), Observations of X-ray and EUV fluxes during X-class solar flares and response of upper ionosphere, *J. Geophys. Res.*, *115*, A12330, doi:10.1029/2010JA015576.

Manju, G., T. K. Pant, C. V. Devasia, S. Ravindran, and R. Sridharan (2009), Electrodynamical response of the Indian low-mid latitude ionosphere to the very large solar flare of 28 October 2003—A case study, *Ann. Geophys.*, *27*, 3853–3860, doi:10.5194/angeo-27-3853-2009.

Mendillo, M., and J. V. Evans (1974), Incoherent scatter observations of the ionospheric response to a large solar flare, *Radio Sci.*, *9*, 197–203, doi:10.1029/RS009i002p00197.

Mendillo, M., et al. (1974), Behavior of the ionospheric *F* region during the great solar flare of August 7, 1972, *J. Geophys. Res.*, *79*, 665–672, doi:10.1029/JA079i004p00665.

Mendillo, M., et al. (2006), Effects of solar flares on the ionosphere of Mars, *Science*, *311*, 1135–1138, doi:10.1126/science.1122099.

Nusinov, A. A. (2006), Ionosphere as a natural detector for investigations of solar EUV flux variations, *Adv. Space Res.*, *37*, 426–432, doi:10.1016/j.asr.2005.12.001.

Ohshio, M. (1971), Negative sudden phase anomaly, *Nature*, *229*, 239–240.

Qian, L., A. G. Burns, P. C. Chamberlin, and S. C. Solomon (2010), Flare location on the solar disk: Modeling the thermosphere and ionosphere response, *J. Geophys. Res.*, *115*, A09311, doi:10.1029/2009JA015225.

Rishbeth, H., and O. K. Garriott (1969), *Introduction to Ionospheric Physics*, Academic, San Diego, Calif.

Smith, F. L., III, and C. Smith (1972), Numerical evaluation of Chapman's grazing incidence integral ch (X, $_{chi}$), *J. Geophys. Res.*, *77*, 3592–3597, doi:10.1029/JA077i019p03592.

Smithtro, C. G., J. J. Sojka, T. Berkey, D. Thompson, and R. W. Schunk (2006), Anomalous F region response to moderate solar flares, *Radio Sci.*, *41*, RS5S03, doi:10.1029/2005RS003350.

Stonehocker, G. H. (1970), Advanced telecommunication forecasting technique in AGY, *AGARD Conf. Proc.*, *29*, 12–27.

Thome, G. D., and L. S. W. Wagner (1971), Electron density enhancements in the E and F regions of the ionosphere during solar flares, *J. Geophys. Res.*, *76*, 6883–6895, doi:10.1029/JA076i028p06883.

Tsurutani, B. T., et al. (2005), The October 28, 2003 extreme EUV solar flare and resultant extreme ionospheric effects: Comparison to other Halloween events and the Bastille Day event, *Geophys. Res. Lett.*, *32*, L03S09, doi:10.1029/2004GL021475.

Wan, W., L. Liu, H. Yuan, B. Ning, and S. Zhang (2005), The GPS measured SITEC caused by the very intense solar flare on July 14, 2000, *Adv. Space Res.*, *36*, 2465–2469, doi:10.1016/j.asr.2004.01.027.

Woods, T. N., S. M. Bailey, W. K. Peterson, S. C. Solomon, H. P. Warren, F. G. Eparvier, H. Garcia, C. W. Carlson, and J. P. McFadden (2003), Solar extreme ultraviolet variability of the X-class flare on 21 April 2002 and the terrestrial photoelectron response, *Space Weather*, *1*(1), 1001, doi:10.1029/2003SW000010.

Woods, T. N., F. G. Eparvier, J. Fontenla, J. Harder, G. Kopp, W. E. McClintock, G. Rottman, B. Smiley, and M. Snow (2004), Solar irradiance variability during the October 2003 solar storm period, *Geophys. Res. Lett.*, *31*, L10802, doi:10.1029/2004GL019571.

Woods, T. N., F. G. Eparvier, S. M. Bailey, P. C. Chamberlin, J. Lean, G. J. Rottman, S. C. Solomon, W. K. Tobiska, and D. L. Woodraska (2005), Solar EUV Experiment (SEE): Mission overview and first results, *J. Geophys. Res.*, *110*, A01312, doi:10.1029/2004JA010765.

Zhang, D. H., and Z. Xiao (2005), Study of ionospheric response to the 4B flare on 28 October 2003 using International GPS Service network data, *J. Geophys. Res.*, *110*, A03307, doi:10.1029/2004JA010738.

Zhang, D. H., Z. Xiao, and Q. Chang (2002), The correlation of flare's location on solar disc and the sudden increase of total electron content, *Chin. Sci. Bull.*, *47*, 82–85, doi:10.1360/02tb9017.

Zhang, D. H., et al. (2006), Study of the response of the ionosphere over sun-lit boundary region to solar flare, Chin. *J. Space Sci.*, *26*, 321–325.

Zhang, D. H., X. H. Mo, L. Cai, W. Zhang, M. Feng, Y. Q. Hao, and Z. Xiao (2011), Impact factor for the ionospheric total electron content response to solar flare irradiation, *J. Geophys. Res.*, *116*, A04311, doi:10.1029/2010JA016089.

Y. Chen, M. He, H. Le, J. Liu, L. Liu, B. Ning, Z. Ren, W. Wan, B. Xiong, and B. Zhao, Beijing National Observatory of Space Environment, Institute of Geology and Geophysics, Chinese Academy of Sciences, Beijing 100029, China. (wanw@mail.iggcas.ac.cn)

Y. Wei, Max-Planck-Institut für Sonnensystemforschung, Katlenburg-Lindau D-37191, Germany.

P. Withers, Center for Space Physics, Boston University, Boston, MA 02215, USA.